Solid Earth Discuss., 5, 427–461, 2013
www.solid-earth-discuss.net/5/427/2013/
doi:10.5194/sed-5-427-2013

Solid Earth
Discussions
Open Access

New constraints on the geometry of the subducting African plate and the overriding Aegean plate obtained from P receiver functions and seismicity

F. Sodoudi[1,2], A. Bruestle[3], T. Meier[4], R. Kind[1,2], W. Friederich[3], and EGELADOS working group

[1]Freie Universität Berlin, Malteserstr. 74–100, 12249 Berlin, Germany
[2]Helmholtz Centre Potsdam, GFZ German Research Centre for Geosciences, Telegrafenberg, 14473 Potsdam, Germany
[3]Ruhr-Universität Bochum, Universitätsstr. 150, 44801 Bochum, Germany
[4]Christian-Albrechts Universität zu Kiel, Otto-Hahn-Platz 1, 24118 Kiel, Germany

Received: 22 March 2013 – Accepted: 25 March 2013 – Published: 16 April 2013

Correspondence to: F. Sodoudi (foroug@gfz-potsdam.de)

Published by Copernicus Publications on behalf of the European Geosciences Union.

Abstract

New combined P receiver functions and seismicity data obtained from the EGELADOS network employing 65 stations within the Aegean constrained new information on the geometry of the Hellenic subduction zone. The dense network and large dataset enabled us to accurately estimate the Moho of the continental Aegean plate across the whole area. Presence of a negative contrast at the Moho boundary indicating the serpentinized mantle wedge above the subducting African plate was clearly seen along the entire forearc. Furthermore, low seismicity was observed within the serpentinized mantle wedge. We found a relatively thick continental crust (30–43 km) with a maximum thickness of about 48 km beneath the Peloponnesus Peninsula, whereas a thinner crust of about 27–30 km was observed beneath western Turkey. The crust of the overriding plate is thinning beneath the southern and central Aegean (Moho depth 23–27 km). Moreover, P receiver functions significantly imaged the subducted African Moho as a strong converted phase down to a depth of 180 km. However, the converted Moho phase appears to be weak for the deeper parts of the African plate suggesting reduced dehydration and nearly complete phase transitions of crustal material into denser phases. We show the subducting African crust along 8 profiles covering the whole southern and central Aegean. Seismicity of the western Hellenic subduction zone was taken from the relocated EHB-ISC catalogue, whereas for the eastern Hellenic subduction zone, we used the catalogues of manually picked hypocenter locations of temporary networks within the Aegean. P receiver function profiles significantly revealed in good agreement with the seismicity a low dip angle slab segment down to 200 km depth in the west. Even though, the African slab seems to be steeper in the eastern Aegean and can be followed down to 300 km depth implying lower temperatures and delayed dehydration towards larger depths in the eastern slab segment. Our results showed that the transition between the western and eastern slab segments is located beneath the southeastern Aegean crossing eastern Crete and the Karpathos basin. High resolution P receiver functions also clearly resolved the top of a strong low

SED
5, 427–461, 2013

velocity zone (LVZ) at about 60 km depth. This LVZ is interpreted as asthenosphere below the Aegean continental lithosphere and above the subducting slab. Thus the Aegean mantle lithosphere seems to be 30–40 km thick, which means that its thickness increased again since the removal of the mantle lithosphere about 15 to 35 Ma ago.

1 Introduction

The tectonics of the Hellenic subduction zone has been controlled since late Cretaceous by the convergence between Africa and Eurasia, the subduction of African oceanic lithosphere beneath the Aegean lithosphere, and the accretion of Africa derived terranes to Eurasia (e.g. Dercourt et al., 1986; Gealey, 1988; Stampfli and Borel 2004). The recent kinematics of the Aegean is characterized by a counterclockwise rotation of the Aegean and the Anatolian plates and internal extension of the plates (e.g. McKenzie, 1972, 1978; LePichon et al., 1995; Cocard et al., 1999; Kahle et al., 1999; McClusky et al., 2000). Subduction of African oceanic lithosphere along the Hellenic arc and its associated roll back is supposed to be the cause of the extension and might contribute to the rotation of the Anatolian–Aegean plate (e.g. LePichon et al., 1995; McClusky et al., 2000). From late Miocene time onward, extensional basins developed in the entire Aegean (e.g. Mascle and Martin, 1990; Brun and Sokoutis, 2010), combined with the propagation of the North Anatolian fault into the Aegean region since about ca. 5 Ma (Armijo et al., 1996; Faccenna et al., 2006). Recent studies showed that stretching of the Aegean lithosphere took place in a distinctly episodic fashion, not in a manner that can be described as continuous or progressive (e.g. Forster and Lister, 2009). Even though, the style of the deformation that accommodates the extension is disputed. Recent seismic anisotropy analysis found evidence for a highly 3-D deformation pattern, strong Miocene extension of the lower crust in the southern Aegean associated with the formation of metamorphic core complexes and significant recent deformation of the entire lithosphere in the northern Aegean (Endrun et al., 2011).

SED
5, 427–461, 2013

High seismic activity occurs along the Hellenic arc (e.g. Papazachos and Comnikakis, 1971; Hatzfeld and Martin, 1992; Knapmeyer, 1999; Papazachos et al., 2000). The depths of the hypocentres increase towards volcanic arc. Depending on location accuracy, seismicity in the Wadati–Benioff zone may provide valuable information on the geometry of the subducting African lithosphere. Interestingly, the Wadati–Benioff zone can only be observed down to about 100 km to 180 km depth and terminates roughly beneath the Hellenic volcanic arc. Therefore, the slab may only be followed towards greater depths by seismic tomography or receiver function studies.

The subducting African lithosphere has been consistently imaged by several tomographic studies using body waves (e.g. Spakman et al., 1988, 1993; Papazachos and Nolet, 1997; Bijwaard et al., 1998; Piromallo and Morelli, 2003; Schmid et al., 2004; Chang et al., 2010; Biryol et al., 2011). Recent tomographic studies showed the Hellenic slab continuously from the surface down to 1400 km and revealed the associated penetration of the slab into the lower mantle (e.g. Chang et al., 2010). The geometry of the Hellenic subduction zone has also been intensely studied by other geophysical methods, but none of them could resolve the subducting slab at depths larger than about 160 km (e.g. Makris and Vees, 1977; Makris, 1978; Knapmeyer and Harjes, 2000; Bohnhoff et al., 2001; Li et al., 2003; Endrun et al., 2004, 2008; Meier et al., 2004; Tirel et al., 2004; Snopek and Casten, 2006). Recent receiver function studies obtained new constraints on the nature of the subducting African plate (e.g. Sodoudi et al., 2006; Gesret et al., 2011). Sodoudi et al. (2006) imaged the bottom of the subducting African lithosphere (LAB) down to 225 km beneath the volcanic arc using S receiver functions. However, the subducting African Moho could not be shown deeper than 160 km beneath the volcanic arc. Surface wave studies could also not image the deeper part of the slab, but they found evidence for the presence of a low velocity asthenosphere beneath the Aegean plate and above the subducting African slab (e.g. Karagianni et al., 2002; Meier et al., 2004; Bourova et al., 2005; Endrun et al., 2008).

Establishment of the temporary, broadband seismic network of EGELADOS (Exploring the Geodynamics of Subducted Lithosphere using an Amphibian Deployment Of

SED
5, 427–461, 2013

Seismographs) within the CRC 526 “Rheology of the Earth” founded by the Deutsche Forschungsgemeinschaft covering the entire Hellenic subduction zone from the Peloponnesus in the west to the western Turkish coast in the east, was carried out by the Ruhr-University Bochum in collaboration with partners at the Aristoteles University of Thessaloniki, the National Observatory Athens, the Technical University of Crete, the Istanbul Technical University, the GFZ Potsdam and the University of Hamburg (Fig. 1). Deploying more than 80 temporary onshore and offshore stations provided a unique opportunity to perform a detailed investigation into the properties of the Hellenic subduction zone and to image crust and mantle structure with high resolution.

In this paper, we employ the P receiver function technique to the temporary land stations and the permanent GEOFON stations. Dense seismic sampling obtained from these stations allows reaching a high resolution image of the descending African plate in the southern and central Aegean. We combine our results with hypocenter locations of the EHB-ISC catalogue for the western Hellenic subduction zone and new accurate hypocenter locations recorded by the temporary CYCNET and EGELADOS networks (Bruestle, 2012) for the eastern Hellenic subduction zone and particularly discuss the correlation of P receiver function images and seismic activity.

2 Data and methodology

The EGELADOS network consists of 56 on- and 24 off-shore stations deployed on the Greek mainland, on most of the southern Aegean islands and in western Turkey from October 2005 to April 2007. 45 of the temporary onshore stations and all offshore stations were equipped by the German amphibian seismograph pool (DEPAS). The remaining temporary stations were provided by Ruhr-University Bochum. Additionally, 22 permanent onshore stations of the Global Seismic Network GEOFON (Geoforschungszentrum Potsdam, Germany), the Hellenic Broadband seismic Network HL (National Observatory Athens NOA, Greece), and the Mediterranean Network MedNet (Instituto Nazionale di Geofisica e Vulcanologia INGV, Italy) were also included to

SED
5, 427–461, 2013

complete the temporary network. We used at least 1.5 yr of teleseismic data recorded at 65 onshore stations (56 temporary and 9 permanent GEOFON stations) to calculate the P receiver functions (Fig. 1). All available events with a magnitude (mb) larger than 5.5 and at a distance of 30–95° were analyzed. Additionally, more than 11 yr of data were available for the permanent GEOFON stations for the P receiver function analysis. We computed P receiver functions for all stations as described by Sodoudi et al. (2006).

To image the seismicity of the Hellenic subduction zone, about 8200 hypocenter locations with a location uncertainty of less than 20 km were selected from various catalogues. Seismicity of the western Hellenic subduction zone (lat < 25°, profiles 1–4 in Fig. 1) was taken from the relocated EHB-ISC catalogue 1960–2007 (Engdahl et al., 1998). Seismicity of the eastern Hellenic subduction zone (lat > 25°, profiles 4–8 in Fig. 1) was taken from catalogues of manually picked hypocenter locations of temporary networks. This dataset consists of about 3000 hypocenter locations (Bruestle, 2012) determined by the temporary EGELADOS network, of about 4000 relocated hypocenter locations (Bruestle, 2012) obtained by the temporary CYCNET network covering the central subdcution zone from 2002–2004 (Bohnhoff et al., 2004, 2006), and of about 2000 hypocenter locations of the temporary LIBNET network (Becker et al., 2009) covering the forearc SE of Crete from 2003–2004 .

3 Observations

Stacked traces of P receiver functions (PRFs) of 65 EGELADOS stations are shown in Fig. 2. They are filtered with a low-pass filter of 1s corner period. At all stations (except forearc stations) we can clearly see a positive P-to-S conversion in the time interval from 2.5 to 6 s delay time (shown in black), which stem from the Moho discontinuity. Furthermore, we observe strong multiple converted phases from the Moho boundary (shown with blue circles). The converted Moho phase as well as its first multiple can be clearly observed beneath the stations located relatively far from the Hellenic trench

SED
5, 427–461, 2013

(see Fig. 1). At the stations located in the forearc of the subduction (marked Forearc in Fig. 2), the converted Moho phase has disappeared and instead a negative phase is seen. Such a reversal of sign for the Moho conversion has been previously observed beneath the Cascadia, Hellenic subduction zones and Central Andes (e.g. Knappmeyer and Harjes, 2000; Bostock et al., 2002; Li et al., 2003; Endrun et al., 2004; Sodoudi et al., 2006, 2011). Clear arrivals of the Moho conversions and of the multiples (Ppps) allowed an accurate estimation of the crustal thickness beneath the whole region. The calculated Aegean Moho depths and Vp/Vs ratios are listed in Table 1.

More detailed images can be provided by our migrated P receiver functions along different profiles covering the whole central and southern Aegean. Figure 3 shows depth migrations of PRFs down to 80 km depth along the eight S–N profiles shown in Fig. 1. In Fig. 3b accurate hypocenter locations of temporary networks catalogues are also shown (profiles 5–8). High frequency P receiver functions reliably indicate the presence of the Aegean and African plates. The continental Moho of the Aegean plate can be well seen beneath the northern part of all profiles up to the forearc area (labeled Moho, see Fig. 3). The thickest crust of about 48 km is observed beneath the Peloponnesus Peninsula, where the Hellenides mountains are located (see profile 1). We found relatively thinner crust of approximately 27–30 km beneath the stations located in Turkey (see profile 8). The crust becomes thinner and is approximately only about 23–27 km thick beneath the southern and central Aegean Sea. Further south, beneath the forearc area, the positive Moho phase is no longer visible and is continued by negative converted phases. This is a common feature, which can be reliably observed beneath the forearc on all profiles. The negative Moho indicates a low velocity zone interpreted as serpentinized mantle wedge above the subducting plate (Sodoudi et al., 2006). Interestingly, this low velocity zone shows also low seismicity, whereas the high seismicity occurs just above or below it. From profile 5 – where accurate locations of seismic events at the seismogenic interface are available (Becker et al., 2009) – it becomes evident that the plate contact between the serpentinized mantle and the subducting plate is mainly aseismic. Thus, the serpentinized mantle wedge is

SED
5, 427–461, 2013

deforming mainly aseismically. On the other hand the seismogenic zone terminates where the serpentinized mantle wedge comes in contact with the plate interface. Meier et al. (2007) noted that the seismogenic zone terminates at the southern coastline of Crete and postulate that the recent uplift of Crete is related to the return flow above the seismically decoupled plate interface. Here we show that the serpentinized mantle wedge is present along the entire forearc of the Hellenic Subduction zone and its location coincides with the location of the forearc high.

Furthermore, the Moho of the subducting African plate (labeled slab) can be also clearly imaged throughout the whole region at depths ranging from 40 to 80 km beneath the forearc area. As Fig. 3b shows, the seismicity (for profiles 5–8) is also consistent with the P receiver function results. Both, the P receiver functions as well as the hypocenter locations constrain the geometry of the slab.

In the next step, to have a clearer image of the subducted African crust, we separately show the stacked PRFs obtained from the western and eastern parts of the Aegean. For the western part we took stations along profiles 1–3 and for the eastern part those along profiles 4–7. Figure 4 illustrates the stacked PRF traces obtained from these two parts. The PRFs are filtered with a low pass of 3 s and sorted by the relative distance of the stations from the Hellenic trench. We show them in a larger time window than in Fig. 2. The most pronounced conversions correspond to the Moho of the subducting African plate (marked slab, red dashed lines). This phase is clearly shown at times ranging from 6 s beneath the forearc region to about 11 s beneath the Peloponnesus (station PE02) for the western Aegean, whereas it can be followed from 5 s under the forearc area to 11 s beneath the volcanic arc (station SANT) for the eastern Aegean. Further north, the continuation of the slab phase is not clear (shown with red dotted lines). Instead, the significant converted phase associated with the continental Aegean Moho (shown as Moho) and its multiple (shown as Moho Multiple) are well imaged.

SED
5, 427–461, 2013

4 Results and discussion

We calculated P-to-S conversion points at 200 km depth using the minimum 1-D-velocity model of Bruestle (2012). For each profile, we considered the PRFs, whose piercing point is located within the data band of 60 km from each side of the profile. Then we stacked them in bins of 4 km and sorted them according to their distance from the starting point of the profile (see Fig. 1). Figure 5 indicates the binned PRFs along the eight profiles shown in Fig. 1. For each profile, local seismicity (Engdahl et al., 1998; Becker et al., 2009; Bruestle, 2012) is overlaid on the PRF data. Generally, there is a good correlation between the geometry of the slab shown by seismicity and that obtained from the PRFs. Both of them can satisfactorily resolve the shallower part of the slab down to at least 90 km (~ 10 s).

Our results together with seismicity enabled us to image the deeper part of the slab with a higher resolution than before, especially for the eastern Hellenic subduction zone, where the resolution of the seismicity of the temporary network catalogues (profiles 5–8) is better than 20 km with an average location error of less than 10 km as estimated by the location routine NonLinLoc (Becker et al., 2009; Bruestle, 2012). Regarding the dominant wave periods of the P wave (approximately 2 s), a maximum depth resolution of about 2 km can be theoretically estimated for P-to-S conversions at discontinuities. Considering some more errors obtained from lateral heterogeneities and noise, we expect to have less than 5 km error in depth estimation. In contrast, resolution of surface wave studies as well as the resolution obtained from tomographic body wave studies is in general lower. Furthermore, previous P receiver function studies could not image the Hellenic slab deeper than 120–160 km depth (Knappmeyer and Harjes, 2000; Li et al., 2003; Endrun et al., 2004; Sodoudi et al., 2006). In this work, especially the comparison of P receiver functions with hypocenters of the Wadati–Benioff Zone allows to distinguish between primary conversions at the top of the slab and multiples of the continental Aegean crust. Multiples could otherwise be misinterpreted as flat slabs.

SED
5, 427–461, 2013

Our results mainly show a relatively shallow dipping slab segment beneath the western part of the Aegean (Fig. 5a). Along profile1 located in the westernmost part of the Aegean, the Moho of the subducting plate is consistently imaged at times ranging from 5 s to about 11 s (Fig. 5a, black dashed line). A single event at 13 s (130 km) depth may reveal the deeper part of the slab. This part is however not well resolved by our PRFs. Beneath profile 2, the seismicity stops at about 12 s. Even though, the continuation of the converted phase from the slab can be observed down to at least 20 s (200 km). This feature can be also clearly seen along profile 3. In contrast to seismicity, which terminates at 11 s, the slab phase is imaged as a downgoing phase to 22 s. Low conversion amplitudes behind the island arc – pointing to reduced contrasts – and the lack of seismicity at depth larger than about 100 km may indicate reduced dehydration and nearly complete phase transitions of crustal material into denser phases like eclogite. There are however indications for weaker conversions down to about 250 km depth. That means the slab seems to continue towards larger depths in accordance with body wave tomography. We note that at larger depths the slab may be formed by continental rather than oceanic lithosphere because according to tectonic reconstructions not more than about 500 km to 700 km of oceanic lithosphere has been subducted at the recent Hellenic arc (Meier et al., 2004; van Hinsbergen, 2005; Brun and Sokoudis, 2010).

The PRFs along profile 4 are significantly different from those observed along profiles 1–3. Besides the shallow dipping western slab segment, which can be shown by the both seismicity and PRFs at times ranging from 5 to 11 s, the PRFs clearly reveal another dominant downgoing phase. This phase may probably be observed to 30 s and shows a larger dip angle (see Fig. 5a). Furthermore, the low dip angle of the western slab segment seems to be continued to 26 s (260 km). Such a downgoing phase can be also significantly resolved beneath profiles 5–6 (Fig. 5b). Here, we deal with two different converted phases. The first one, which correlates generally well with seismicity, is observed to 25 s (250 km depth). However, the latter one shows a larger dip angle and can be followed down to at least 30 s (300 km). Thus profiles 5–6 image

SED
5, 427–461, 2013

the transition from the western to the eastern segment of the slab that is dipping more steeply and can be imaged deeper.

Along profile 7, where the most seismicity occurs down to depths of about 180 km, we can only observe the steeper eastern slab segment. The low dip angle western slab segment may not be identified any more. PRFs along Profile 8 could significantly show the slab phase down to 12 s. However, the continuation of the slab phase is not clear but may be visible to 30 s. We converted times into the depth domain using the minimum 1-D-velocity model of Bruestle (2012). The results derived from the migrated PRF data are shown for profiles 5 and 7 located in the eastern and easternmost Aegean, respectively (Fig. 6a and b). The presence of two different segments of the subducting African plate (western and eastern segments) is clearly shown beneath the profile 5, whereas beneath the easternmost Aegean (profile 7), the slab seems to have a single steep segment in good agreement with the high seismicity observed beneath this area.

Based on our results we found evidence for a shallow dipping segment beneath the western Aegean (profile 1–3) down to 200–250 km, whereas the eastern segment seems to be steeper and deeper than the western segment and can be significantly resolved down to 300 km (profile 7). Beneath the middle profiles (4–6), the both segments can be clearly observed in the PRF data. Comparing the maximum depth of the seismicity and the maximum depth of observed PRFs we can conclude that dehydration and phase transitions in the crust of the slab are delayed towards larger depths in the eastern segment.

Wortel and Spakman (2000) proposed a horizontal tear within the subducting slab propagating from the southernmost Dinarides southwards towards the western Hellenic subduction. In our analysis we don't find evidence for a horizontally propagating tear beneath Peloponnesus in the region of the western segment of the Hellenic subduction zone. If present, the horizontal tear is confined to the northern Hellenides beneath mainland Greece north of the Peloponnesus and the Golf of Corinth.

Based on regional body-wave travel-time tomography Papazachos and Nolet (1997) found also evidence for a western and eastern slab segment and noted that at about

SED
5, 427–461, 2013

200 km depth the western and eastern slab segments meet along a rather sharp edge with a right angle. Analyzing hypocenters of the relocated EHB-ISC catalogue (Engdahl et al., 1998) Meier et al. (2007) identified the two slab segments and proposed that they are associated with laterally varying properties of the African slab. Furthermore, in the Mediterranean southeast of Crete, Rhodes and south of western Anatolia, high velocities in the mantle lithosphere – typical for cold oceanic lithosphere – are found by tomographic studies (Bijward et al., 1998; Marone et al., 2004; Erduran et al., 2008; Legendre et al., 2012), whereas south of Peloponnesus and western Crete velocities in the mantle lithosphere are lower (Meier et al., 2004; Legendre et al., 2012). Our high resolution images and the precise event locations reveal the geometry of the two segments down to about 300 km depth. The larger dip angle of the eastern segment may be associated with lower slab temperatures and dehydration delayed towards larger depths. Based on the PRFs the transition between the two segments is located beneath profiles 5 and 6 crossing eastern Crete and the Karpathos basin east of Karpathos. In addition, in accordance with the observations by Papazachos and Nolet (1997) our receiver function images seem to indicate an increase of the dip of the western slab segment at about 70 km depth (9 s) on profiles 2 and 3. This may be indicative for an increased continental character of the western slab segment towards shallower depths.

Furthermore, high frequency PRF data have enabled us to resolve another dominant positive phase at 15–17 s (Fig. 5, shown with blue dashed line, marked as 2). This phase is clearly seen beneath the northern part of all profiles and seems to be parallel to the Moho phase. However, this phase is not a Moho multiple due to its arrival time. The Moho multiple comes just before this phase (red dashed line). To model this phase, synthetic P receiver functions are obtained from forward modelling. We started with the minimum 1-D velocity model obtained by joint inversion for event locations (Bruestle, 2012). Synthetics are computed by iteratively fitting the modeled waveform to the observed data utilizing a non-linear least-squares approach. For this purpose we stacked data from the northern part of profile 5, where this phase is clearly imaged. As

SED
5, 427–461, 2013

Fig. 7a shows, a simple model containing a Moho at 25 km as a sharp crust-mantle boundary can reproduce a pronounced positive signal (at 2.5 s) and two multiples (at 10.5 and 13 s) in the P receiver function that fits well the observed stacked data. Even though, the positive signal at 16.5 s cannot be produced by this model. Modeling shows that a velocity reduction (∼ 8 %) below 60 km produces an additional negative signal at about 6 s (Fig. 7b). Furthermore, this Low Velocity Zone (LVZ) also provides a positive multiple phase arriving at 16.5 s delay time. The presence of the strong negative converted phase at 6–8 s (Fig. 5, shown with black dotted line, marked as 1) just below the Moho phase is observed beneath all profiles. Thus, our results imply a low-velocity layer below about 60 km depth. That means a LVZ between the Aegean Moho and the high velocities of the African slab is required beneath the northern parts of all profiles (central Aegean).

Low velocities below 60 km depth beneath the southern Aegean and the volcanic arc have also been observed by P-wave tomography (Drakatos et al., 1997; Papazachos and Nolet, 1997). In addition, surface wave dispersion analysis revealed also a low-velocity layer with minimum velocities of 4.15 $\mathrm{km\,s^{-1}}$ at depths of 50–80 km between the Aegean Moho and the slab in the Sea of Crete and beneath the Cyclades (Endrun et al., 2008). An even more pronounced low-velocity layer was found by Bourova et al. (2005). They observed a large low-velocity anomaly at a depth of 50–100 km beneath the prolongation of the North Anatolian Trough in the northern Aegean, where strong deformation is currently observed at the surface.

We have observed the top of the LVZ at about 60 km beneath the back arc area (central Aegean), where no estimation of the lithospheric thickness was made before. The observed LVZ has been constrained consistently over a dense network of receivers in the Aegean and mainland Greece between the Moho of the Aegean plate and the slab. Our result confirms the previous results and provides excellent new information on the LVZ beneath the central Aegean. Our LVZ is seen slightly deeper (∼ 10 km) than that observed in the Sea of Crete and beneath the southern Aegean, but its depth is

SED
5, 427–461, 2013

consistent with the depth derived from P-wave tomography and surface wave analysis in the northern Aegean.

In good agreement with Endrun et al. (2008), we interpret this negative discontinuity at 60 km depth as the lithosphere-asthenosphere boundary (LAB) of the continental Aegean plate. This is a remarkable result as it indicates a very thin mantle lithosphere in the central and northern Aegean and furthermore a relatively sharp LAB (~ 8 % velocity reduction). Taking the error bounds of P receiver functions (±5 km) into account, we found a relatively thicker lithosphere in the central Aegean (60 km) rather than that seen by surface waves analysis beneath the southern Aegean between forearc and volcanic arc (40–50 km). Given a crustal thickness of about 23–27 km in the central Aegean, the mantle lithosphere is only about 30–40 km thick. Although there is evidence for lithospheric stretching during the extensional processes governing the more recent (last 30 Ma) evolution of the Aegean, the interpretation of a thinned mantle lithosphere would imply a greater thickness of the mantle lithosphere before 30 Ma. Instead, a detachment of the mantle lithosphere beneath the accreted continental terranes has been proposed for the Aegean in order to explain the rather continuous slab (Meier et al., 2004), nappe stacking and metamorphism in the Aegean (van Hinsbergen et al., 2005; Jolivet and Brun, 2010). Similarly, delamination of the Anatolian mantle lithosphere has been proposed by Keskin (2003). The removal of the mantle lithosphere of accreted continental terranes would mean that despite of the lithospheric extension the mantle lithosphere has gained again a thickness of about 30–40 km in the central Aegean since its removal about 35 Ma to 15 Ma ago. Processes involved in the evolution of a younger mantle lithosphere may be cooling of the asthenospheric mantle, magmatic underplating, dehydration of serpentinized mantle, or chemical differentiation of crustal material (Artemieva and Meissner, 2012).

Our recent S receiver function analysis (Sodoudi et al., 2006) provided earlier constraints on the LAB in the Aegean. The S receiver function data resolved LAB signals at about 170 km beneath mainland Greece and at 130 km beneath western Turkey (Fig. 8). Due to the locations of the EGELADOS stations we could not provide any

SED
5, 427–461, 2013

estimation of the Aegean LAB beneath mainland Greece in this work. Furthermore, for the central Aegean, no S receiver function data are available yet.

We show in Fig. 8 stacked PRFs obtained from the boxes located beneath the northern parts of the study area, where the negative phase at 6–8 s was significantly observed in our PRFs (Fig. 8a, see also Fig. 5). We combined our results with those recently shown by Sodoudi et al. (2006) using S receiver functions. Stacked PRFs computed for each box (see Fig. 8a) are illustrated along a W-E trending profile covering the central Aegean. We also included the stacked SRFs obtained from five boxes mostly located beneath the mainland Greece and western Turkey from Sodoudi et al. (2006). As Fig. 8b shows, the LAB signal is found at 6–8 s beneath the central Aegean in the PRFs. The P and S receiver functions yield consistent results for the LAB signal if multiples in the P receiver functions are carefully identified (compare box 3 with box 4 and box 6 with box 7). Beneath mainland Greece the LAB is found at about 17 s (~ 170 km). This can be seen in box 1, 2, 3 and may be also indentified at 20 s in box 4 (Fig. 8). This signal indicates very likely the bottom of the subducting lithosphere as the Moho of the subducting plate is found at about 100 km (12–14 s) depth in the region of boxes 1, 2 (Fig. 5a). Thus in agreement with Sodoudi et al. (2006) we can provide good depth estimation of the African LAB beneath western Aegean. Furthermore, the signal at about 10 s (~ 100 km) in box 8 showing the Aegean LAB in western Anatolia would imply a thickening of the Aegean lithosphere towards Anatolia.

5 Conclusions

We analyzed more than 1.5 yr of teleseismic data recorded by 65 temporary and permanent stations of EGELADOS network. By combining P receiver function observations and new accurate locations of seismic events, we could obtain a high-resolution image of the subducting African plate beneath the continental Aegean plate in the southern and central Aegean. Observation of the negative Moho velocity contrast of the Aegean plate along the entire forearc clearly showed the serpertinized mantle wedge

SED
5, 427–461, 2013

over the subducted African plate. Furthermore, the plate contact between the serpentinized mantle and the subducting plate seems mainly to be aseismic. We could also constrain accurate crustal thicknesses and Vp/Vs ratios for the continental Aegean plate, since it could be sampled at the spacing of the EGELADOS stations. We identified the thickest crust of about 48 km beneath the Peloponnesus Peninsula, whereas a relatively thinner crust of about 27–30 km was observed beneath the western Turkey. The crust of the Aegean plate was estimated to be 23–27 km thick beneath the southern and central Aegean. Our PRFs could also significantly image the Moho of the subducting African plate as a strong converted phase in excellent agreement with the spatial distribution of the earthquake hypocenters. We compared PRFs to hypocenters of the relocated EHB-ISC catalogue (Engdahl et al., 1998) beneath the western Aegean. In the southeastern Aegean, PRFs were compared with microseismicity obtained from the accurate located EGELADOS and relocated CYCNET catalogues (Bruestle, 2012) as well as accurate locations from the LIBNET network (Becker et al., 2009). The geometry of the subducted African plate was imaged along eight different profiles covering the southern and central Aegean. Our results mainly resolved a low dip angle slab segment down to 200–250 km depth beneath the western Aegean, whereas we reliably found a steeper and deeper slab segment down to at least 300 km beneath the south eastern Aegean. This observation may support lower slab temperatures and delayed dehydration and phase transitions within the oceanic crust towards larger depths in the eastern segment. Furthermore, we estimated the transition between the two segments beneath the southeastern Aegean crossing eastern Crete and the Karpathos basin. Based on our high-frequency PRFs, we found a clear indication of the presence of the LAB beneath the continental Aegean plate. The LAB of the Aegean plate was clearly seen as a relatively sharp boundary (velocity drop of 8 %), which lies at a depth of 60 km beneath the central Aegean. If only crustal material has been accreted to Eurasia due to the collision of Gondwana derived terranes this implies a growths of the Aegean mantle lithosphere of about 30–40 km in the last about 15 Ma to 35 Ma.

SED
5, 427–461, 2013

Acknowledgements. Mobile seismic stations for the temporary networks were provided by the DEPAS and GIPP pools (GFZ Potsdam, AWI Bremerhaven). Furthermore, we thank NOA, Greece, GFZ Potsdam, and INGV, Rome, for data of permanent seismic networks. Funding was provided by the German Research Foundation in the framework of the Collaborative Research Centre 526 "Rheology of the Earth " and by GFZ Potsdam. Synthetic S receiver functions have been computed using *SeisPy* – Seismological Python: a Python extension package for seismological analysis by J. Saul, GFZ Potsdam.

References

Armijo, R., Meyer, B., King, G., Rigo, A., and Papanastassiou, D.: Quaternary evolution of the Corinth Rift and its applications for the late Cenozoic evolution of the Aegean, Geophys. J. Int., 126, 11–53, 1996.

Becker, D., Meier, T., Bohnhoff, M., and Harjes, H.-P.: Seismicity at the convergent plate boundary offshore Crete, Greece, observed by an amphibian network, J. Seismol., 14, 369–392, doi:10.1007/s10950-009-9170-2, 2009.

Bijwaard, H., Spakman, W., and Engdahl, E. R.: Closing the gap between regional and global travel time tomography, J. Geophys. Res., 103, 30055–30078, 1998.

Biryol, C. B., Beck, S. L., Zandt, G., and Özacar, A. A.: Segmented African lithosphere beneath the Anatolian region inferred from teleseismic P-wave tomography, Geophys. J. Int., 184, 1037–1057, 2011.

Bohnhoff, M., Makris, J., Papanikolaou, D., and Stavrakakis, G.: Crustal investigation of the Hellenic subduction zone using wide aperture seismic data, Tectonophysics, 343, 239–262, 2001.

Bohnhoff, M., Rische, M., Meier, T., Endrun, B., Harjes, H. P., and Stavrakakis, G.: CYC-NET: a temporary seismic network on the Cyclades (Aegean Sea, Greece), Seismol. Res. Lett., 75, 352–357, 2004.

Bohnhoff, M., Rische, M., Meier, T., Becker, D., Stavrakakis, G., and Harjes, H. P.: Microseismic activity in the Hellenic Volcanic Arc, Greece, with emphasis on the seismotectonic setting of the Santorini-Amorgos zone, Tectonophysics, 423, 17–33, 2006.

Bostock, M. G., Hyndman, D., Rondeny, S., and Peacock, S. M.: An inverted continental Moho and serpentinization of the forearc mantle, Nature, 417, 536–538, 2002.

SED

5, 427–461, 2013

Bourova, E., Kassara, I., Pedersen, H. A., Yanovskaya, T., Hatzfeld, D., and Kirtazi, A.: Constraints on absolute S-wave velocities beneath the Aegean Sea from surface wave analysis, Geophys. J. Int., 160, 1006–1019, 2005.

Brun, J.-P. and Sokoutis, D.: 45 m.y. of Aegean crust and mantle flow driven by trench retreat, Geology, 38, 815–818, doi:10.1130/G30950.1, 2010.

Bruestle, A.: Seismicity of the eastern Hellenic Subduction Zone, PhD thesis, Ruhr-Universität Bochum, 2012.

Chang, S. J., van der Lee, S., Flanagan, M. P., Bedle, H., Marone, F., Matzle, E. M., Pasyanos, M. E., Rodgers, A. J., Romanowicz, B., and Schmid, C.: Joint inversion for three-dimensional S velocity mantle structure along the Tethyanmargin, J. Geophys. Res., 115, B08309, doi:10.1029/2009JB007204, 2010.

Cocard, M., Kahle, H. G., Peter, Y., Geiger, A., Veis, G., Felekis, S., Paradissis, D., and Billiris, H.: New constraints on the rapid crustal motion of the Aegean region: recent results inferred from GPS measurements (1993–1998) across the West Hellenic Arc, Greece, Earth Planet. Sc. Lett., 172, 39–47, 1999.

Dercourt, J., Zonenshain, L. P., Ricou, L. E., Kazmin, V. G., Le Pichon, X., Knipper, A. L., Grandjacquet, C., Sbortshikov, I. M., Geyssant, J., Lepvrier, C., Pechersky, D. H., Boulin, J., Sibuet, J. C., Savostin, L. A., Sorokhtin, O., Westphal, M., Bazhenov, M. L., Lauer, J. P., and Biju-Duval., B.: Geological evolution of the Thetys belt from the Atlantic to the Pamirs since the Lias, Tectonophysics, 123, 241–315, 1986.

Drakatos, G., Karantonis, G., and Stavrakakis, G. N.: P-wave crustal tomography of Greece with use of an accurate two-point ray tracer, Ann. Geofis., XL, 25–36, 1997.

Endrun, B., Meier, T., Bischoff, M., and Harjes, H. P.: Lithospheric structure in the area of Crete constrained by receiver functions and dispersion analysis of Rayleigh phase velocities, Geophys. J. Int., 158, 592–608, doi:10.1111/j.1365-246X.2004.02332.x, 2004.

Endrun, B., Meier, T., Lebedev, S., Bohnhoff, M., Stavrakakis, G., and Harjes, H. P.: S velocity structure and radial anisotropy in the Aegean region from surface wave dispersion, Geophys. J. Int., 174, 593–616, 2008.

Endrun, B., Lebedev, S., Meier, T., Tirel, C., and Friederich, W.: Complex layered deformation within the Aegean crust and mantle revealed by seismic anisotropy, Nat. Geosci., 4, 203–207, doi:10.1038/ngeo1065, 2011.

SED
5, 427–461, 2013

Engdahl, E. R., Van Der Hilst, R. D., and Buland, R.: Global teleseismic earthquake relocation with improved travel times and procedures for depth relocation, B. Seismol. Soc. Am., 88, 722–743, 1998.

Faccenna, C., Bellier, O., Martinod, J., Piromallo, C., and Regard, V.: Slab detachment beneath eastern Anatolia: a possible cause for the formation of the North Anatolian fault, Earth Planet. Sc. Lett., 242, 8–97, 2006.

Forster, M. and Lister, G.: Core-complex-related extension of the Aegean lithosphere initiated at the Eocene-Oligocene transition, J. Geophys. Res., 114, B02401, doi:10.1029/2007JB005382, 2009.

Gealey, W. K.: Plate tectonic evolution of the Mediterranean-Middle East region, Tectonophysics, 155, 285–306, 1988.

Gesret, A., Laigle, M., Diaz, J., Sachpazi, M., Charalampakis, M., and Hirn, A.: Slab top dips resolved by teleseismic converted waves in the Hellenic subduction zone, Geophys. Res. Lett., 38, L20304, doi:10.1029/2011GL048996, 2011.

Hatzfeld, D. and Martin, C.: The Aegean intermediate seismicity defined by ISC data, Earth Planet. Sc. Lett., 113, 267–275, 1992.

Jolivet, L. and Brun, J.-P.: Cenozoic geodynamic evolution of the Aegean, Int. J. Earth Sci., 99, 109–138, doi:10.1007/s00531-008-0366-4, 2010.

Kahle, H. G., Cocard, R., Peter, Y., Geiger, A., Reilinger, R., McClusky, S., King, R., Barka, A., and Veis, G.: The GPS strain rate field in the Aegean Sea and western Anatolia, Geophys. Res. Lett., 26, 2513–2516, 1999.

Karagianni, E. E., Pabagiotopoulos, D. G., Panza, G. F., Suhadolc, P., Papazachos, C. B., Papazachos, B. C., Kirtazi, A., Hatzfeld, D., Makropoulos, K., Priestley, K., and Vuan, A.: Rayleigh wave group velocity tomography in the Aegean area, Tectonophysics, 358, 187–209, 2002.

Keskin, M.: Magma generation by slab steepening and breakoff beneath a subduction-accretion complex: an alternative model for collision-related volcanism in eastern Anatolia, Turkey, Geophys. Res. Lett., 30, 8046, doi:10.1029/2003GL018019, 2003.

Knapmeyer, M.: Geometry of the Aeagean Benioff zones, Ann. Geofis., 42, 27–38, 1999.

Knapmeyer, M. and Harjes, H.-P.: Imaging crustal discontinuities and the down-going slab beneath western Crete, Geophys. J. Int., 143, 1–21, 2000.

SED
5, 427–461, 2013

Legendre, C., Meier, T., Lebedev, S., Friederich, W., and Viereck-Götte, L.: A shear-wave velocity model for the European upper mantle from automated inversion of seismic shear and surface waveforms, Geophys. J. Int., 191, 282–304, 2012.

Le Pichon, X., Chamot-Rooke, N., and Lallemant, S.: Geodetic determination of the kinematics of central Greece with respect to Europe: implications for eastern Mediterranean tectonics, J. Geophys. Res., 100, 12675–12690, 1995.

Li, X., Bock, G., Vafidis, A., Kind, R., Harjes, H.-P., Hanka, W., Wylegalla, K., Van der Meijde, M., and Yuan, X.: Receiver function study of the Hellenic subduction zone: imaging crustal thickness variations and the oceanic Moho of the descending African lithosphere, Geophys. J. Int., 155, 733–748, 2003.

Makris, J.: The crust and upper mantle of the Aegean region from deep seismic soundings, Tectonophysics, 46, 269–284, 1978.

Makris, J. and Vees, R.: Crustal structure of the central Aegean Sea and the islands of Evia and Crete, Greece, obtained by refractional seismic experiments, J. Geophys., 42, 330–341, 1977.

Marone, F., Van der Lee, S., and Giardini, D.: Three-dimensional uppermantle S-velocity model for the Eurasia–Africa plate boundary region, Geophys. J. Int., 158, 109–130, doi:10.1111/j.1365-246X.2004.02305.x, 2004.

Mascle, J. and Martin, L.: Shallow structure and recent evolution of the Aegean Sea: a synthesis based on continuous reflection profiles, Mar. Geol., 94, 271–299, 1990.

McClusky, S., Balassanian, S., Barka, A., Demir, C., Ergintav, S., Georgiev, I., Gurkan, O., Hamburger, M., Hurst, K., Kahle, H., Kastens, K., Kekelidze, G., King, R., Kotzev, V., Lenk, O., Mahmoud, S., Mishin, A., Nadariya, M., Ouzounis, A., Paradissis, D., Peter, Y., Prilepin, M., Reilinger, R., Sanli, I., Seeger, H., Tealeb, A., Toksöz, M. N., and Veis, G.: Global Positioning System constrains on plate kinematics and dynamics in the eastern Mediterranean and Caucasus, J. Geophys. Res., 105, 5695–5719, 2000.

McKenzie, D.: Active tectonics of the Mediterranean region, Geophys. J. Roy. Astr. S., 30, 109–185, 1972.

McKenzie, D.: Active tectonics of the Alpine–Himalayan belt: the Aegean Sea and surrounding regions, Geophys. J. Roy. Astr. S., 55, 217–254, 1978.

Meier, T., Dietrich, K., Stöckhert, B., and Harjes, H. P.: 1-dimensional models of the shear-wave velocity for the eastern Mediterranean obtained from the inversion of Rayleigh wave phase velocities and tectonic implications, Geophys. J. Int., 156, 45–58, 2004.

SED
5, 427–461, 2013

Meier, T., Becker, D., Endrun, B., Rische, M., Bohnhoff, M., Stöckhert, B., and Harjes, H. P.: A model for the Hellenic subduction zone in the area of Crete based on seismological investigations, in: The Geodynamics of the Aegean and Anatolia, edited by: Taymaz, T., Yilmaz, Y., and Dilek, Y., Geol. Soc. Spec. Publ., 291, 1, 183–199, 2007.

Papazachos, B. C. and Comninakis, P. E.: Geophysical and tectonic features of the Aegean arc, J. Geophys. Res., 76, 8517–8533, 1971.

Papazachos, C. B. and Nolet, G.: P and S deep velocity structure of the Hellenic area obtained by robust nonlinear inversion of travel times, J. Geophys. Res., 102, 8349–8367, 1997.

Papazachos, B. C., Karakostas, V. G., Papazachos, C. B., and Scordilis, E. M.: The geometry of the Wadati–Benioff zone and lithospheric kinematics in the Hellenic arc, Tectonophysics, 319, 275–300, 2000.

Piromallo, C. and Morelli, A.: P wave tomography of the mantle under the Alpine–Mediterranean area, J. Geophys. Res., 108, 2065, doi:10.1029/2002JB001757, 2003.

Schmid, C., Van Der Lee, S., and Giardini, D.: Delay times and shear wave splitting in the Mediterranean region, Geophys. J. Int., 159, 275–290, 2004.

Snopek, K. and Casten, U.: 3GRAINS: 3-D gravity interpretation software and its application to density modeling of the Hellenic subduction zone, Comput. Geosci., 32, 592–603, doi:10.1016/j.cageo.2005.08.008, 2006.

Sodoudi, F., Kind, R., Hatzfeld, D., Priestley, K., Hanka, W., Wylegalla, K., Stavrakakis, G., Vafidis, A., Harjes, H. P., and Bohnhoff, M.: Lithospheric structure of the Aegean obtained from P and S receiver functions, J. Geophys. Res., 111, B12307, doi:10.1029/2005JB003932, 2006.

Sodoudi, F., Yuan, X., Asch, G., and Kind, R.: High-resolution image of the geometry and thickness of the subducting Nazca lithosphere beneath northern Chile, J. Geophys. Res., 116, B04302, doi:10.1029/2010JB007829, 2011.

Spakman, W., Wortel, M. J. R., and Vlaar, N. S.: The Hellenic subduction zone: a tomographic image and its geodynamical implications, Geophys. Res. Lett., 15, 60–63, 1988.

Spakman, W., Van der Lee, S., and Van der Hilst, R. D.: Travel time tomography of the European-Mediterranean mantle down to 1400 km, Phys. Earth Planet. In., 79, 3–73, 1993.

Stampfli, G. M. and Borel, G. D.: The transmed transect in space and time: constraints on the paleotectonic evolution of the mediterranean domain, in: The TRANSMED Atlas: the Mediterranean Region from Crust to Mantle, edited by: Cavazza, W., Roure, F., Spakman, W., Stampfli, G. M., and Ziegler, Springer Verlag, Berlin, 53–80, 2004.

SED
5, 427–461, 2013

Tirel, C., Gueydan, F., Tiberi, C., and Brun, J.-P.: Aegean crustal thickness inferred from gravity inversion, geodynamical implications, Earth Planet. Sc. Lett., 228, 267–280, doi:10.1016/j.epsl.2004.10.023, 2004.

Van Hinsbergen, D. J. J., Hafkenscheid, E., Spakman, W., Meulenkamp, J. E., and Wortel, R.: Nappe stacking resulting from subduction of oceanic and continental lithosphere below Greece, Geology, 33, 325–328, 2005.

Wortel, R. and Spakman, W.: Subduction and slab detachment in the Mediterranean-Carpathian region, Science, 290, 1910–1917, 2000.

SED

5, 427–461, 2013

Table 1. Stations, their coordinates, observed arrival times of the Moho and Moho multiple (Ppps) of the Aegean plate and their corresponding Moho depths and Vp/Vs ratios.

Station	Lat.	Lon.	Moho time (s)	Moho Multiple time (s)	Moho depth (km)	Vp/Vs
Tur4	37.0800	27.8077	3.5	12	27	1.74
AT01	38.06	24.3784	2.3	9	21.5	1.62
KIMO	36.7949	24.5680	2.3	7.5	17	1.8
ANID	36.6251	25.6847	2.4	9.5	23	1.61
IOSI	36.7347	25.3618	2.7	10.5	25	1.62
NAXO	36.9800	25.4400	2.5	9.2	21.5	1.67
SERI	37.1610	24.4853	2.7	10	23	1.67
IKAR	37.6435	26.3050	2.7	10	23	1.67
FOLE	36.6216	24.9197	3	10	22.5	1.78
KEAI	37.6232	24.3191	2.9	11.6	28	1.6
NEAK	36.4087	25.4014	2.85	11.4	27	1.6
ANAF	36.3581	25.7783	2.9	11.4	27	1.62
AMOS	36.7956	25.7690	3.1	11	25	1.71
SCHI	36.8744	25.5180	3	10.3	23	1.74
AMOE	36.9150	25.9788	2.9	10.8	25	1.66
ANPA	37.0323	25.0763	2.9	10	23	1.74
PARS	37.0285	25.2253	2.9	10.6	24.5	1.68
SYRO	37.4569	24.9266	2.9	10.5	24	1.69
MYKO	37.4822	25.3844	2.8	11.2	27	1.6
ANDR	37.8361	24.9482	2.7	10.8	26	1.6
AT02	38.0473	23.8638	2.8	11	26	1.61
TUR6	37.0159	28.4262	3.3	11.4	26	1.74
TUR8	36.8273	28.9390	3.2	11.5	26.5	1.7
TUR5	37.0302	27.3167	3.3	11.7	27	1.71
KOSI	36.7449	26.9517	3	11.4	27	1.65
LERO	37.1634	26.8353	3.1	11.5	27	1.67
TUR2	37.6420	27.2418	3.3	11.8	27	1.7
TUR3	37.4663	27.5380	3.5	11.1	24	1.83
TUR1	38.0865	26.8676	3.2	11.4	26	1.7
SAMO	37.7043	26.8377	3.4	12	27.5	1.71
TUR7	36.7017	27.5697	3.8	13.5	31	1.7
TUR9	36.7015	28.0887	3.5	12	27	1.74
TILO	36.4485	27.3535	3.4	11	24	1.8
ASTY	36.5795	26.4114	3.4	10.5	23	1.86
PARO	37.1150	25.1825	3.3	10.4	23	1.84
APE	37.0689	25.5306	3.4	10.9	24	1.82
PE07	37.1478	22.8195	3.5	12.1	27.5	1.73
AT03	38.268	23.4677	3.8	12	26	1.84
AT04	37.7252	24.0496	3.5	13	30	1.67
SANT	36.371	25.459	4	14.1	32	1.71
PE01	38.0170	22.0283	4.3	13.5	29.5	1.84
PE02	37.8958	22.4907	6	21	48	1.72
PE08	36.8311	22.4420	4.3	14.8	33.5	1.74
IDHR	37.3908	23.2591	4.1	13.3	29.5	1.8
PE04	37.6007	22.9593	4.8	16.2	36	1.76
PE05	37.5128	22.4553	5	18.2	42	1.68
PE03	37.3784	21.7722	4.5	15.5	35	1.74

SED
5, 427–461, 2013

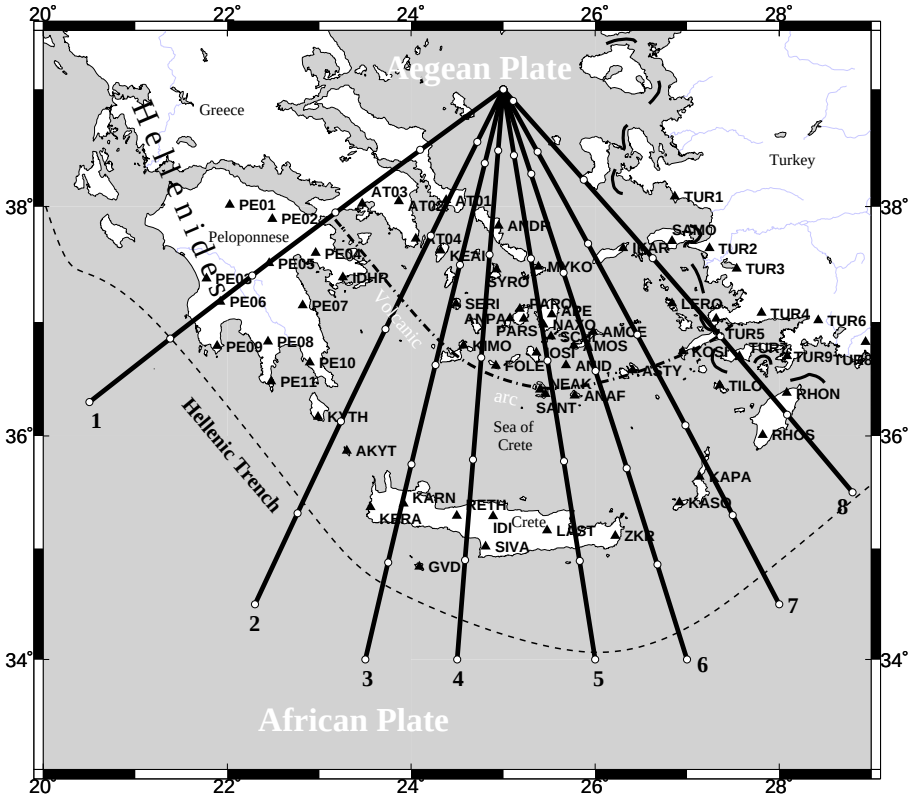

Fig. 1. Distribution of the EGELADOS stations used for receiver function technique (black triangles). Location of the Hellenic trench is shown with black dashed line. Dashed-dotted line denotes location of the volcanic arc. Black solid lines indicate the positions of eight S–N trending profiles used for P receiver functions. Small white circles on the profile lines mark 100 km distance interval.

SED
5, 427–461, 2013

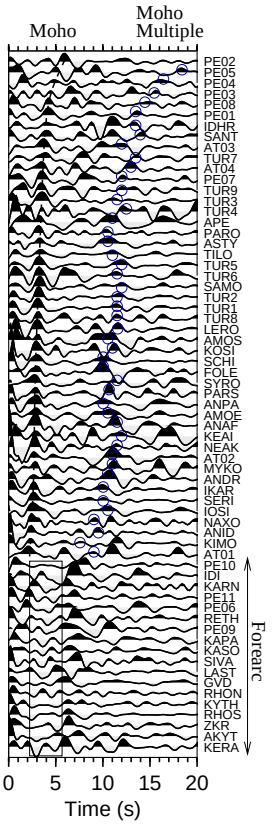

Fig. 2. Stacked PRFs of 65 EGELADOS stations. Stations (except stations in the forearc) are sorted according to the arrival time of the Aegean Moho phase from 2.3 to 6 s (black dashed line). They are filtered using a low-pass filter of 1s. No clear positive P-to-S conversions from the Aegean Moho can be seen for the forearc stations (black box). Arrival times of the Aegean Moho phases and Moho multiples (Ppps, blue circles) are used to calculate the Moho depth and Vp/Vs beneath each station (see Table 1).

SED
5, 427–461, 2013

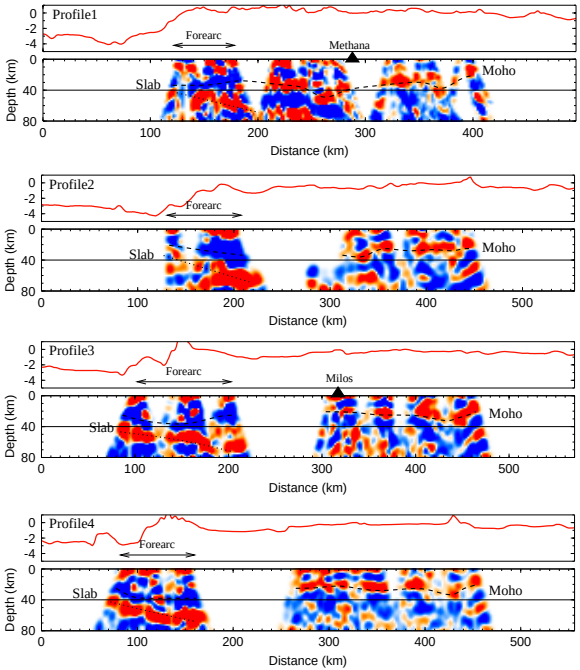

Fig. 3a. (Caption on next page.)

SED
5, 427–461, 2013

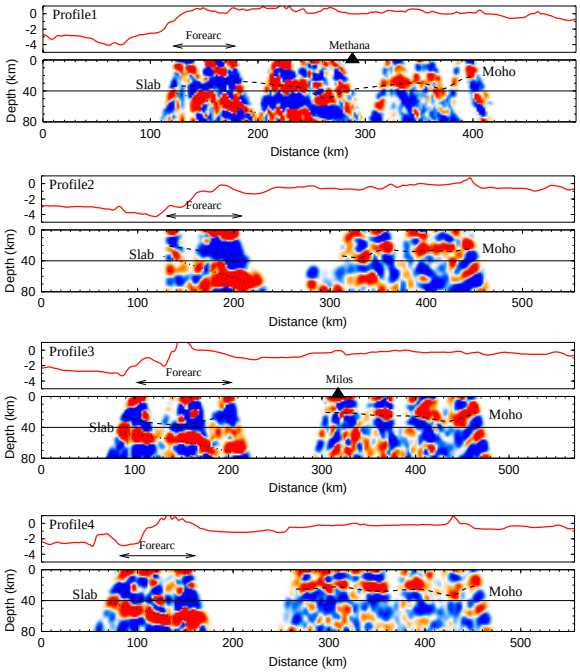

Fig. 3b. Migrated PRFs along S–N trending profiles shown in Fig. 1. Topography is shown at the top. Positive (negative) phases are shown in red (blue). Positions of the volcanoes are shown with black triangles. **(a)** For the western profiles (1–4): the Moho of the continental Aegean plate (labeled Moho) is well observed beneath the whole profiles up to the forearc region. This phase is not visible beneath the forearc area and seems to be continued as negatively converted phases. The subducted African Moho (labeled Slab) is well observed beneath the forearc area at depths ranging from 40 to 80 km. Note that the thickest crust of about 48 km is seen beneath the Peloponnesus (profile 1). **(b)** Same as **(a)** for the eastern profiles (5–8). The black circles show the seismicity of the temporary network catalogues (Becker et al., 2009; Bruestle, 2012). Note that the most seismicity occurs above or below the serpentinized mantle wedge (negative phases) seen beneath the forearc area.

SED
5, 427–461, 2013

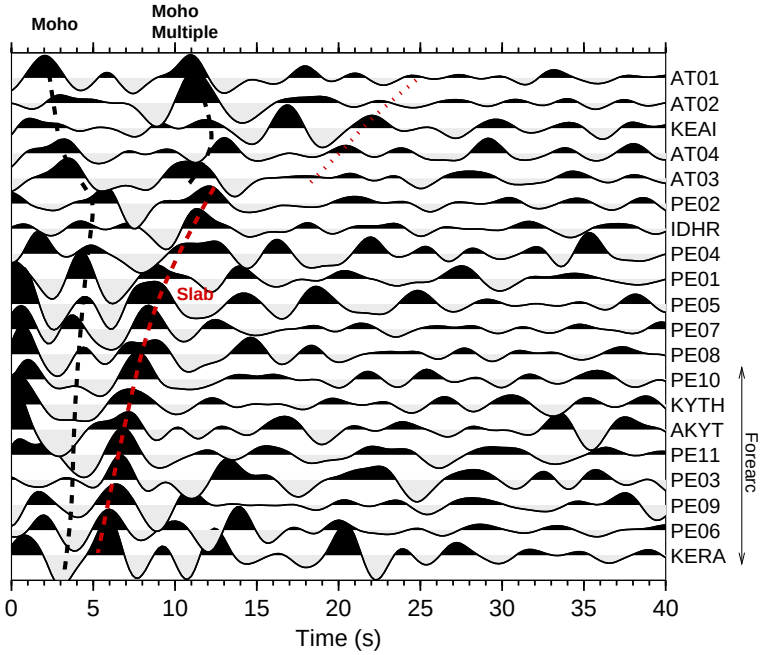

Fig. 4a. (Caption on next page.)

SED
5, 427–461, 2013

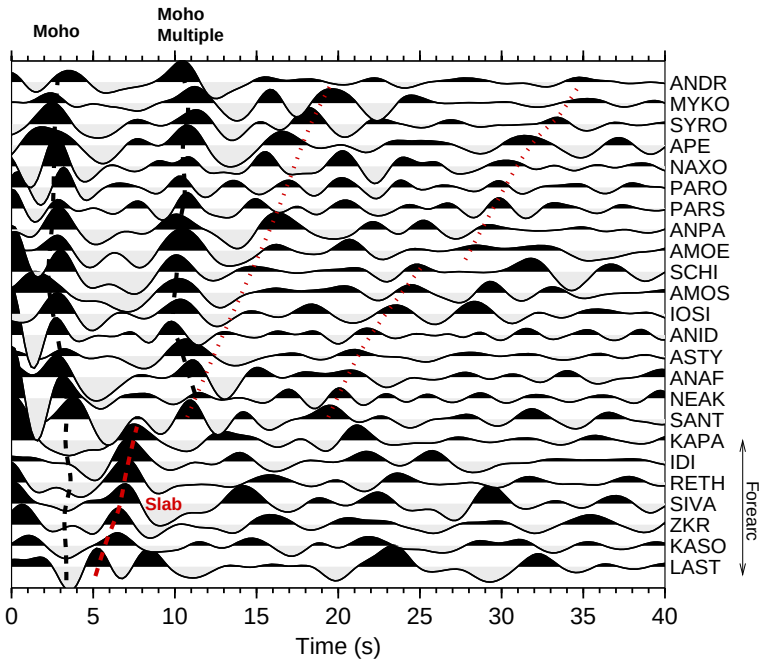

Fig. 4b. Stacked PRFs sorted by their relative distance from the Hellenic trench from south to north. They are filtered with a band-pass of 3–20 s. **(a)** The western Aegean profiles 1–3 stacked into one profile: the converted phase from the continental Aegean Moho and its multiple can be clearly observed beneath all stations except those located in the forearc (shown with black dashed lines). The converted phase from the subducting African Moho is well seen down to 12 s beneath the northern Peloponnesus (shown with red dashed line). Further north, the continuation of this phase is not clear (red dotted line). **(b)** Same as **(a)** for the eastern Aegean (profiles 4–7): the subducting African Moho phase can be followed to 11 s beneath the volcanic arc (station SANT). Further north, two different phases may be visible to 20 and 35 s, respectively (red dotted lines).

SED
5, 427–461, 2013

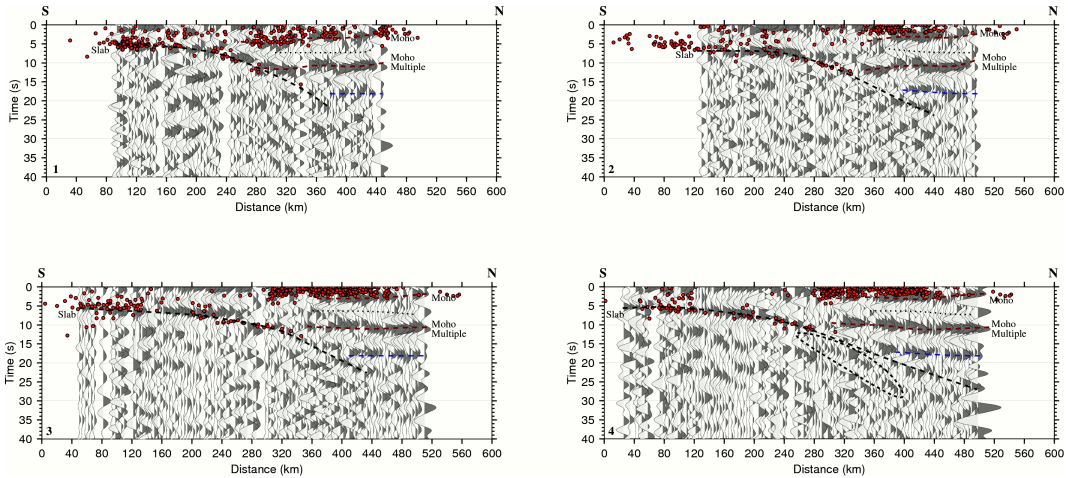

Fig. 5a. (Caption on next page.)

SED
5, 427–461, 2013

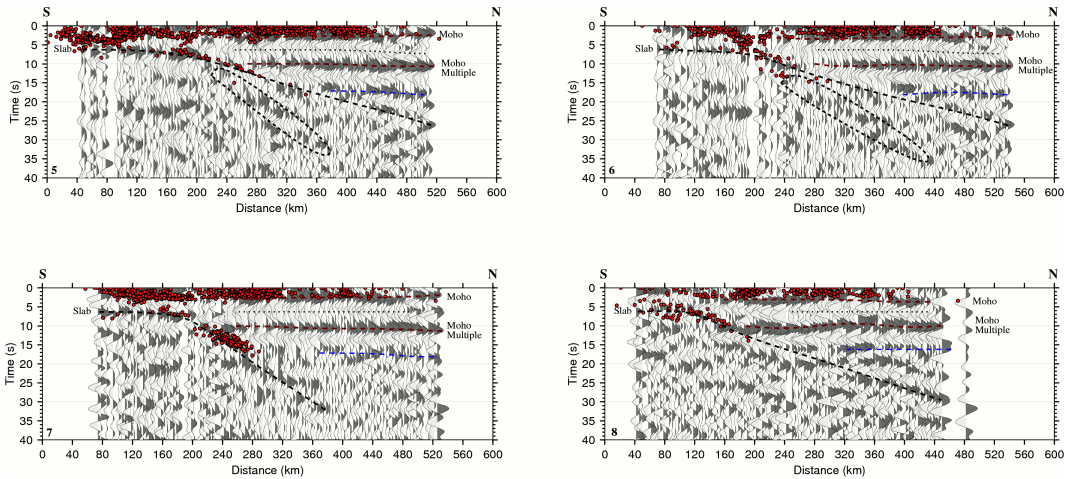

Fig. 5b. Sections obtained from the binned PRF data (in 4 km bins) along profiles shown in Fig. 1. Seismicity is also overlaid on the PRF sections (small red circles). The data are filtered with a band-pass filter of 4–30 s. **(a)** The western Aegean (profiles 1–4). Besides the clear Aegean Moho phase and its multiple (red dashed lines), the downgoing African Moho is also well imaged by PRFs. The PRFs are well correlated with the seismicity of the relocated EHB-ISC catalogue (Engdahl et al., 1998). The Moho phase of the subducted African plate seems to be followed to 20 s for profiles 1–3. Beneath profile 4, two downgoing phases are probably observed (black dashed lines). **(b)** Same as **(a)** for the eastern Aegean (profiles 5–7), but seismicity taken from the temporary network catalogues (Becker et al., 2009; Bruestle, 2012). The same feature as seen beneath profile 4 can be observed beneath the profiles located in the middle part of the Aegean (profile 5–6), whereas the PRFs beneath the easternmost Aegean (profile 7) show a steeper downgoing phase to about 30 s. Note that the strong conversion at 15–17 s (blue dashed lines, marked as 2) may show a multiple phase of the LVZ detected at 6–8 s delay time (shown with black dotted lines, marked as 1).

SED
5, 427–461, 2013

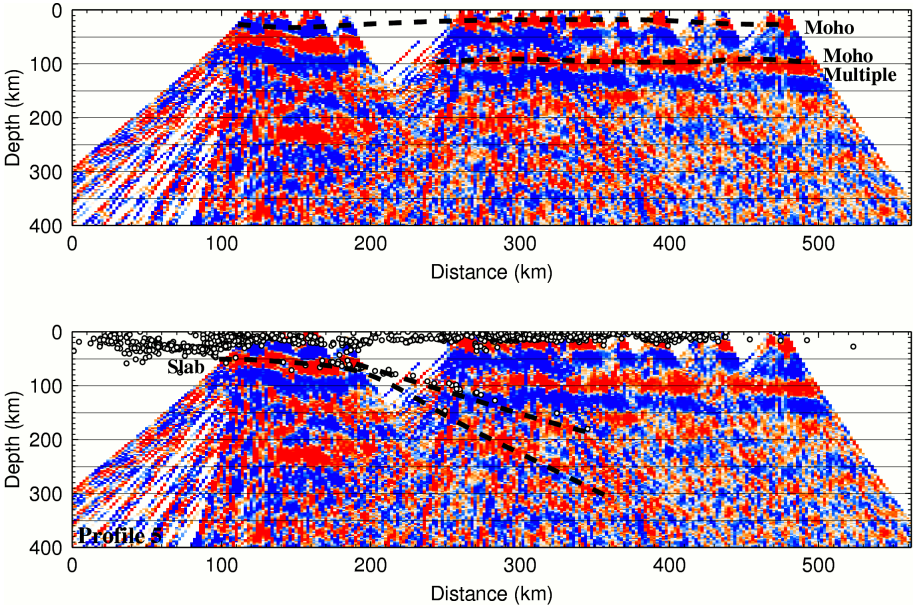

Fig. 6a. (Caption on next page.)

SED
5, 427–461, 2013

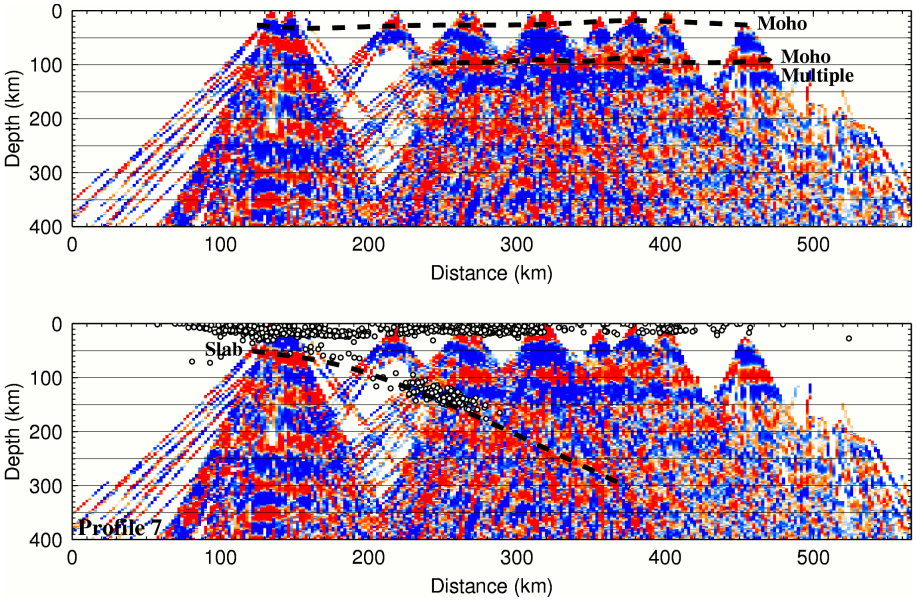

Fig. 6b. Imaged structures obtained from the migrated PRFs without (upper panel) and with seismicity (lower panel) **(a)** Profile 5. Presence of two different segments of the subducting African plate can probably be identified beneath the eastern Aegean (labeled slab, black dashed lines in the lower panel). **(b)** Migrated PRFs for profile 7 located in the easternmost part of the Aegean significantly resolve one segment of the subducting African plate down to a depth of 300 km.

SED
5, 427–461, 2013

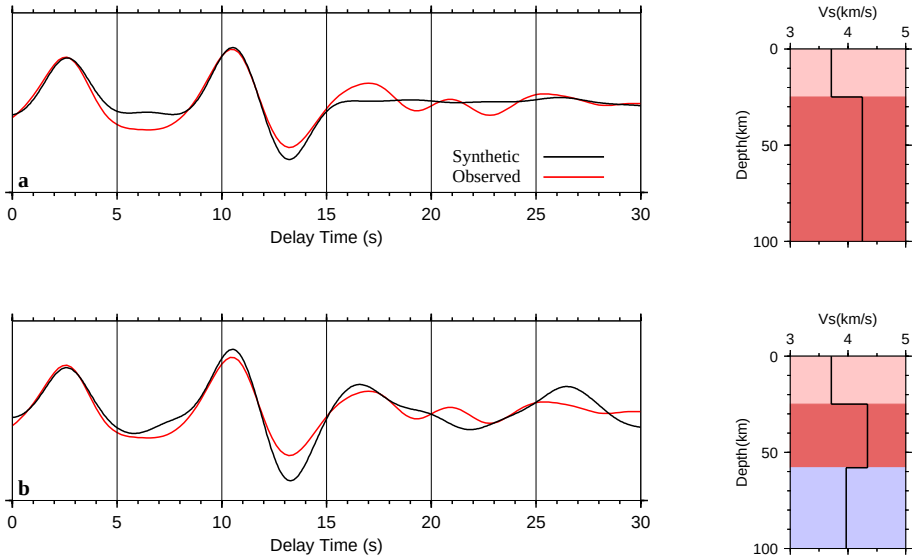

Fig. 7 . Synthetic PRFs calculated to reconstruct the strong positive phase at 15–17 s seen beneath the central Aegean (see Fig. 5). **(a)** A simple model consisting of a strong crust-mantle boundary at 25 km can reproduce the Moho phase and its multiples but cannot constrain the strong positive phase resolved at 16.5 s. **(b)** Adding a LVZ into the model at about 60 km may produce a multiple phase arriving at about 16.5 s.

SED
5, 427–461, 2013

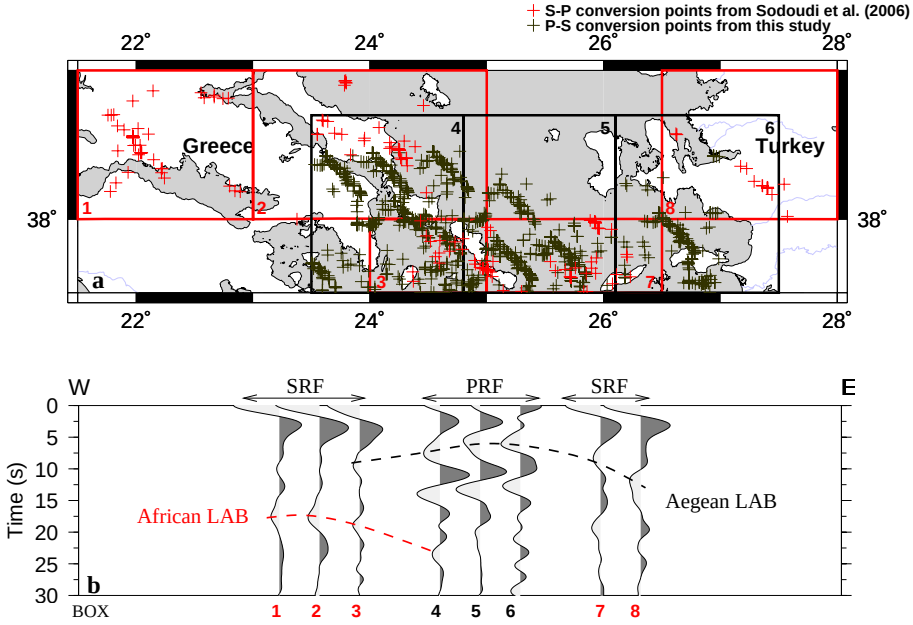

Fig. 8 . Aegean LAB as seen by PRFs from this study compared with the results obtained from SRFs by Sodoudi et al. (2006). **(a)** location of P-to-S (black crosses) and S-to-P (red crosses) piercing points. Red boxes (black boxes) show where the SRFs (PRFs) are considered to be stacked. **(b)** Summation traces of P and S receiver functions obtained from the boxes shown in **(a)**. The Aegean LAB lies at about 6–8 s beneath the central Aegean with a significant deepening to about 10 s towards Turkey. The African LAB lies at about 17 s beneath mainland Greece and western Aegean.

SED
5, 427–461, 2013